AIMS Environmental Science

AIMS Environmental Science, 5(3): 195–215.
DOI: 10.3934/environsci.2018.3.195
Received: 30 April 2018
Accepted: 18 June 2018
Published: 25 June 2018

http://www.aimspress.com/journal/environmental

Research article

Limited impact of sulfate-driven chemistry on black carbon aerosol aging in power plant plumes

Milos Z. Markovic[1,2,4], Anne E. Perring[1,2], Ru-Shan Gao[1], Jin Liao[1,2,5], Andre Welti[1,2,6], Nick L. Wagner[1,2], Ilana B. Pollack[1,2,7], Ann M. Middlebrook[1], Thomas B. Ryerson[1], Michael K. Trainer[1], Carsten Warneke[1,2], Joost A. de Gouw[1,2], David W. Fahey[1,2], Philip Stier[3] and Joshua P. Schwarz[1,*]

[1] Earth System Research Laboratory, Chemical Sciences Division, NOAA, Boulder, Colorado, USA
[2] Cooperative Institute for Research in Environmental Sciences (CIRES), University of Colorado, Boulder, Colorado, USA
[3] Department of Physics, University of Oxford, Oxford, Oxfordshire, United Kingdom
[4] Now at Picarro Inc, Santa Clara, CA, USA
[5] Now at Atmospheric Chemistry and Dynamics Laboratory, NASA Goddard Space Flight Center, Greenbelt, Maryland, and Universities Space Research Association, GESTAR, Columbia, Maryland
[6] Now at Finnish Meteorological Institute, Helsinki, Finland
[7] Now at Department of Atmospheric Science, Colorado State University, Ft. Collins, Colorado, USA

*** Correspondence:** Email: joshua.p.schwarz@noaa.gov; Tel: +13034974637.

Abstract: The aging of refractory black carbon (rBC) aerosol by sulfate-driven chemistry has been constrained in coal-fired power-plant plumes using the NOAA WP-3D research aircraft during the Southern Nexus (SENEX) study, which took place in the Southeastern US in June and July of 2013. A Single Particle Soot Photometer (SP2) determined the microphysical properties of rBC-containing particles including single-particle rBC mass and the presence and amount of internally-mixed non-rBC material, hereafter referred to as "coatings". Most power-plant influenced air was associated with very slightly increased amounts of non-refractory material, likely sulfate internally mixed with the rBC, however this increase was statistically insignificant even after semi-Lagrangian exposure for up to 5 h. On average, the increase in coating thickness was 2 ± 4 nm for particles containing 3–5 fg rBC. Similarly, the number fraction of rBC-containing particles that could be identified as internally mixed was increased by plume chemistry by only 1.3 ± 1.3%. These direct measurements of microphysical aging of rBC-containing aerosol by power plant emissions constrain the enhancement of sulfate chemistry on both rBC's column-integrated absorption optical depth, and rBC-containing aerosol's ability to act as cloud

condensation nuclei. Appling Mie and κ-Köhler theories to the SP2 observations, permits the resulting effect on rBC ambient light-absorption to be capped at the 2–6% level.

Keywords: black carbon aerosol; sulfate chemistry; aerosol aging; sulfate

Abbreviations: AE: absorption enhancement factor; CF: coated number fraction; CT: coating thickness (nm); fg: femtogram; m: meter; MMR: mass mixing ratio; OA: organic aerosol; OOA: oxygenated organic aerosol; PSL: polystyrene latex sphere; rBC: refractory black carbon; SENEX: Southeast Nexus Experiment; SP2: single particle soot photometer; VOC: volatile organic carbon; W: watt

1. Introduction

Atmospheric refractory black carbon (rBC) aerosol warms Earth's climate through absorption of solar radiation in the visible and ultraviolet wavelengths [1–3], and causes an estimated total global radiative forcing of 0.64 W m^{-2} [4]. Regional climate forcing of rBC can be much larger (e.g., 20 W m^{-2} or more over parts of India [5,6]). rBC is emitted into the atmosphere from incomplete combustion of fossil and biofuel, and from biomass burning [7]. Hence, many rBC sources are strongly linked to anthropogenic activity, and are being considered for inclusion in near-term mitigation strategies [7–10]. The relative importance of rBC to climate forcing could increase in the future according to projected emission scenarios [11].

Freshly emitted fossil fuel rBC is typically hydrophobic at emission, and is relatively free of non-refractory material (i.e., is externally mixed) [12]. Exposure in the atmosphere leads to accumulation of non-refractory species such as sulfate and organic aerosol (OA) on the rBC component [9], affecting rBC microphysics including optical properties and interactions with water vapor [13]; these processes are what we term "microphysical aging" (here, simply "aging"). The climate impacts of rBC, which depend in part on its size distribution, vertical gradient, mixing state, and abundance relative to co-emitted species such a sulfate [7,9,14], are not well constrained, and contribute nearly 0.5 W m^{-2} uncertainty to the overall understanding of global climate forcing [4].

The rate of aging of rBC is quite variable not only because of the spatial and temporal variability in the abundance and size distribution of rBC particles, but also because of variability in co-emitted chemical species, in the oxidative capacity of the atmosphere, and in meteorological conditions. Here internally mixed materials are generically referred to as "coatings", while the rBC component is called a "core", without implying any specific morphological information. Subramanian et al. [15] found that the age of an air mass does not necessarily correlate with increase in the amount of coatings associated with rBC cores.

Mixing state can impact the direct radiative forcing of aerosol rBC in two opposing ways: (i) internally mixed chemical species may enhance the absorption of solar radiation by the rBC fraction (the so-called "lensing" enhancement) [2,16–21] even as single-scatter albedo also increases [22], and (ii) internally mixed rBC associated with non-absorbing chemical species such as sulfate is expected to be more hydrophilic and to lead to reduced atmospheric lifetime due to increased deposition [23–27].

Based on recent modeling and laboratory studies, the instantaneous forcing of rBC is believed to be ~50% enhanced by internal mixing [28–32]. Estimates from field measurements suggest a

wider range of values for absorption enhancements by this mechanism. Schwarz et al. [33] deduced from aircraft measurements of rBC mass and mixing state that the presence of non-absorbing coatings can enhance light absorption by the ambient rBC column over the tropics by 30%. Lack et al. [34] showed that internal mixing of rBC with OA and nitrate enhanced absorption of visible radiation in a biomass burning plume in rural Colorado by 38%. Wang et al. [35] suggested that in a polluted urban atmosphere in China, the addition of mainly organic coatings increased the mass absorption cross section of rBC by as much as 80%. On the other side, Cappa et al., [36] found significantly a lower absorption enhancement of rBC (AE_{rBC}) of ~6% in urban-influenced air in California without any correlation to the photochemical age of the air mass. Lan et al. [37] showed that mass absorption enhancements of rBC due to internal mixing was low in an urban plume of a Chinese megacity with a campaign average absorption amplification of 7%.

In addition to uncertainties associated with the absolute impacts of internal mixtures on rBC optics, there is considerable additional uncertainty about the time scales for such aging to occur, and their integrated impact on rBC forcing. Modeling work by Fierce et al. [38] indicated that the aging time scales of rBC can vary from hours to weeks depending on parameters such as the light flux and hygroscopicity of secondary aerosol, and the size of rBC cores undergoing aging. Stier et al. [14] performed a model study that found that coatings could also enhance removal of rBC, countering their impact on optics, and that these two competing mechanisms have different impacts on the rBC burden and optical properties depending on the geographical proximity to source regions. That study predicted that in the southeastern U.S., and most continental areas in close proximity to source regions, anthropogenic sulfur emissions (specifically) would increase the atmospheric aerosol absorption optical depth by 10–30% despite decreasing the atmospheric burden of rBC by 10–20%. Despite the importance of rBC in climate forcing, there is a paucity of systematic investigations of the interactions between rBC and non-refractory chemical species such as sulfate or OA in real atmospheric conditions. Additional modeling and comprehensive field assessments are needed to improve the understanding of the effect of mixing state of rBC on its radiative properties and hence the overall climate forcing.

The SouthEast NEXus (SENEX) field campaign was a large-scale, collaborative project that took place in the Southeastern United States in June and July of 2013 [39]. The goal of SENEX was to investigate the evolution of biogenic and anthropogenic gases and aerosols in this region, and to explore the formation of haze. The US Southeast is characterized by some of the highest levels of sulfate and OA in the nation paired with highly humid conditions [40–47], while the summer-time measurements occurred when photochemical reactions are very important. Numerous state-of-the-science analytical instruments were deployed onboard NOAA WP-3D research aircraft.

Parts of the SENEX flights were designed to sample urban outflows, shale development regions, and various emission point sources—including a focus on the atmospheric impacts of contemporary coal-fired power plants. In developed countries such as the U.S., these do not emit significant amounts of primary ash or rBC particles, but are major sources of carbon dioxide (CO_2), sulfur dioxide (SO_2), and nitrogen oxides (NO_x) [48,49]. The emitted SO_2 can rapidly oxidize to sulfuric acid (H_2SO_4) in the presence of OH radicals and especially hydrogen peroxide in the plume [50]. The resulting H_2SO_4 has low vapor pressure and can nucleate to form ultrafine sulfate particles (SO_4^{2-}) or condense onto preexisting particles [51]. Hence, ultrafine particles are generally present in coal-fired power plant plumes in high concentrations [52,53]. Recent modeling work has shown that new particle formation, and hence particle number in plumes, increases with an increase in mixing ratios

of both SO_2 and NO_x (under low-NO_x background conditions), and decreases with increases in background aerosol concentrations [54]. The inverse relationship between new particle formation and background aerosol is expected due to the competition between nucleation and condensation of vapors onto pre-existing aerosol.

Here we investigate interactions between rBC-containing aerosol particles and coal-fired power plant emissions using measurements collected during the larger SENEX campaign. Observations of the amount of internally mixed material (coating thickness) on rBC, assumed due to daytime sulfate-driven chemistry, are used to constrain enhanced aging of rBC in coal-fired power plant plumes, and to evaluate increased aerosol absorption optical depth due to rBC mixing with sulfate in the Southeast U.S.

2. Materials and methods

In situ measurements of atmospheric particulate and gas pollutants, meteorology, and radiation were made from the NOAA WP-3D research aircraft during the SENEX study. Here we focus on power-plant emissions observed on five research flights of 17 total carried out of the Smyrna/Rutherford County airport in Smyrna, TN, U.S. from June 10 to July 10 of 2013. The study covered a sampling area spanning 31.4°N–42.1°N latitude and 95.0°W and 75.6°W longitude. Most of sampling was within the planetary boundary layer with some excursions of up to 6.5 km above sea level.

The measurements of ambient rBC, which we describe using the nomenclature suggested in Petzold et al. [55], were made with a NOAA SP2 sampling at a flow rate of 2 cm^3 s^{-1} [56,57]. The SP2 utilizes laser-induced incandescence to quantify the mass of refractory rBC (vaporizes at temperatures >4000 K) in single particles with rBC mass corresponding to 80–550 nm volume-equivalent diameters for assumed density of 1.8 g cm^{-3}, independent of particle morphology and mixing state [58]. Upon vaporization of rBC, emitted visible and near-visible thermal radiation are detected with two photomultiplier tube detectors (PMTs) with different wavelength ranges of sensitivity. The rBC composition is constrained with a color-temperature measurement [59]. Additionally, the laser light (λ = 1064) scattered by rBC-containing particles throughout their interaction with the laser was detected using avalanche photodiode detectors. Mass mixing ratios (MMRs) of rBC were calculated by integrating the mass of rBC in individual particles sampled in a volume of ambient air in 1 s and then scaling upward by factor of 1.05–1.15 on a flight-to-flight basis, to account for accumulation-mode rBC mass outside of the SP2 detection range. This was done following widely used approach in Schwarz et al. [59]. Only cloud–free air was analyzed, to ensure avoidance of inlet artifacts [60]. A cloud probe (Model LWS 485, Droplet Measurement Technology, Boulder, CO, U.S.) was used to identify cloud free air samples [61]. The SP2 was calibrated for rBC mass measurements by measuring size-selected (aerodynamic diameter of 125–250 nm) fullerene soot particles (Alfa Aesar, Lot # F12S011, Woodbridge, MA, U.S.); this is the calibration material accepted by the SP2 community for ambient measurements [62], and relied on the mass-to-mobility relationships for this specific material found in Moteki and Kondo [63] and Gysel et al. [64]. A total of four rBC calibrations of SP2 were performed during the study showing that instrument response was stable within 5% in rBC mass over the calibrations. The NOAA SP2 has a near-linear response to rBC mass over a majority of the particle accumulation mode mass range. The SP2 scattering measurements were calibrated with 220 nm polystyrene latex (PSL) spheres before each flight. We associate a total absolute uncertainty of 30% with the rBC MMR.

The number fraction of rBC that can be identified as coated (i.e., internally mixed), and the estimated coating thickness associated with particles with a narrow range of rBC mass content, were calculated as described in Schwarz et al. [33] for particles with rBC-components in the 150–175 nm volume-equivalent diameter range (3–5 fg rBC-mass). The total optical size of these particles was determined using the "leading-edge only" (LEO) fit method [65]. For this size range, there were good particle statistics and the SP2 optically sized the majority (>90%) of rBC-containing particles, reducing analysis biases. We were not able to size rBC-containing particles smaller than these without significant bias, and larger particle concentrations were significantly lower, reducing any utility due to statistical limitations. Mie theory core-and-shell modeling was used to translate the optical size of the particle, combined with the rBC mass content, and assumed indices of refraction, into "coating thickness" of the internal mixture. Although the absolute uncertainty in this measure can be quite high (especially for rBC-containing particles internally mixed with small fractions of non-rBC material), here we are concerned primarily with the precision of the technique, which is dependent on statistics (which are presented with results), and largely independent of the particular assumptions made about indices of refraction. Using the SP2-determined coating thicknesses, the sensitivity of the system merely for identifying internal mixtures (for the number-fraction of internally mixed rBC-containing particles) is estimated to be equivalent to a 25 nm coating thickness. Shell-and-core theory was also utilized to estimate the enhancements in rBC absorption from lensing effects of coatings. κ-Köhler theory was used to estimate water-uptake by rBC-containing particles as described in Schwarz et al. [13]. Here, to deal with ammonium, sulfate and OA mixed in coatings, a volume-weighted hygroscopicity parameter, κ, was used as described by Petters and Kreidenweis [66].

The instrumentation suite of the NOAA P3 is broadly described in an overview article [39]. Here, we use chemical composition of non-refractory aerosol from an aerosol mass spectrometer (AMS, 50% uncertainty, Aerodyne Research, Billerica, MA, U.S.) [67,68]; fine particle number concentrations from a nucleation-mode aerosol size spectrometer (NMASS, 26% uncertainty) [69], and an ultra high sensitivity aerosol spectrometer (UHSAS, Droplet Measurement Technology Inc., Boulder, CO, U.S.) [70]; nitrogen monoxide (NO, 3% uncertainty), nitrogen dioxide (NO_2, 4% uncertainty), and total reactive nitrogen oxides (NO_y, 12% uncertainty) mixing ratios from a chemiluminescence instrument [71–73]; CO (5% uncertainty) from a fluorescence instrument [74]; and SO_2 mixing ratios (20% uncertainty) from a modified Thermo-Environmental Model 43C-TL instrument. The rBC data was time-synchronized with CO to account for differing time delays in sampling. Throughout this manuscript, all error estimates (± 1σ) represent one standard deviation of the mean unless stated otherwise.

The work presented here focuses rBC aging in coal-fired power plant plumes. The gas and aerosol measurements acquired during 5 daytime flights (06/11, 06/16, 06/22, 06/23, and 06/26) were utilized to study rBC aging in 6 plumes of 5 different coal-fired power plants: E. C. Gaston (G, Shelby county, AL), Harllee Branch (HB, Putnam county, GA), Scherer (S, Monroe county, GA), Harding Street (H, Marion county, IN), and Independence (I, Independence county, AR). The secondary fuel types for I and G were residual oil and diesel oil, respectively. The 6 investigated power plant plumes were selected from 14 plumes sampled throughout the campaign based on meeting all of the following criteria: (i) a distinct enhancement of SO_2 in the plume over the surrounding (background) air was observed; (ii) SO_2 and NO_y mixing ratios maximized in the closest plume intercept downwind of a power plant and then decreased with age of the plume due to dilution, chemical transformation, and dry deposition (i.e., the plume evolved without the injection of

subsequent emissions downwind); (iii) the bulk mass loadings of sulfate increased downwind of a power plant due to oxidation of SO_2 to H_2SO_4, and H_2SO_4 condensation and coagulation, (iv) there were negligible emissions of rBC from the power plants, and (v) the flights were carried out during the days when photo-chemistry occured. These conditions were selected specifically to allow investigation of changes in rBC microphysical properties in a "natural laboratory".

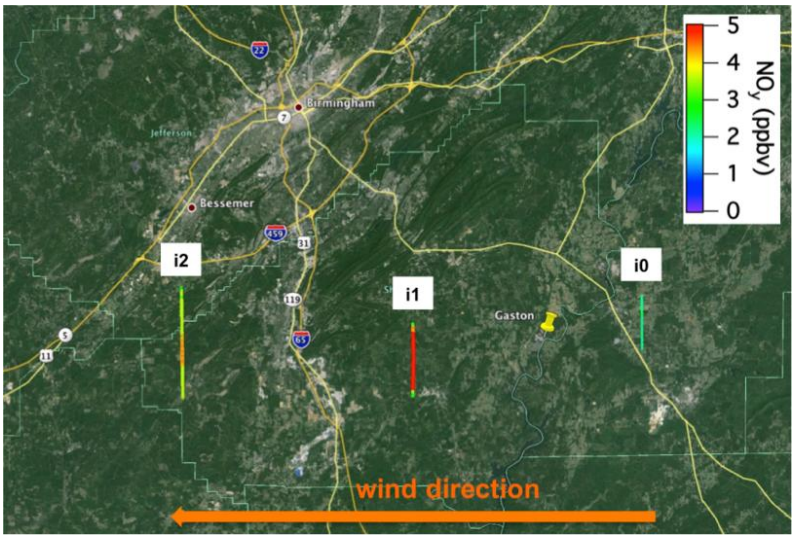

Figure 1. The map of the E. C. Gaston coal-fired power plant plume intercepts during the RF07 on June 22, 2013. The plume intercepts are colored by NO_y mixing ratio. The color scale was cut off at 5 ppbv for clarity, so that the red color represents NO_y values ≥5 ppbv. The wind direction (easterly) is indicated with an orange arrow.

3. Results and discussion

3.1. Identification of coal-fired power plant plumes and rBC aging precursors

The E. C. Gaston power plant plume sampled on Saturday, June 22 2013 provided the clearest example of enhanced aging of rBC, and hence is used as a case study to illustrate our methods and results. A map of the plume-perpendicular transects colored as a function of NO_y volume mixing ratio is shown in Figure 1. The plume transects show large enhancements of NO_y and SO_2 mixing ratios relative to the surrounding air mas (Figure S1). In this case the wind direction was easterly, with low and relatively constant wind speeds in the range of 2.5–3.0 m s^{-1}. Wind speed coupled with distance from each given power plant were used to calculate the respective ages for all plume-perpendicular transects discussed in this manuscript. The WP-3D flew ~ 13 km upwind (~1.5 hr air transport time) of the power plant to sample the background air mass (notated "i0"), and then intercepted the plume twice downwind of the power plant. The first plume intercept was 17.6 km (~1.7 hr, i1) downwind of the power plant and 13.8 km east and upwind of Interstate 65 in the region south of Birmingham, AL. The second plume intercept (i2) was 48.2 km (~5.0 hr) downwind of the power plant, and 16 km west and downwind of Interstate 65. Although Interstate 65 was located between the first and the second plume intercepts, insignificant amounts of rBC and CO from traffic were mixed into the power plant plume, as shown in Figure 2; the stability of rBC concentrations in

both plume intercepts downwind of the power plant were similar to those in the background, also indicating that that the power plant did not emit rBC. Further, any freshly emitted rBC would decrease observed internal mixing with rBC, as fresh emissions tend to consist mostly of bare rBC compared to backgrounds; there was no sign of reductions in coated number fraction. This allowed for the investigation of the aging of rBC in actual field conditions rather than those of a flow reactor. In this setting an air mass containing regional rBC population was "spiked" with known levels of NO_y and SO_2 and was chemically aged.

Compared to the regional background value of 1.9 ± 0.1 ppbv in i0, the mixing ratio of NO_y increased to 8.0 ± 3.6 ppbv in i1 due to power plant stack emissions, and then decreased to 3.7 ± 0.4 ppbv in i2 as the plume was subjected to dilution and NO_y was lost to deposition, particle formation or other processes (Figure 2). Although the measurements of SO_2 across the upwind transect (i0) were unavailable due to an automated instrument calibration, mixing ratio changes similar to those observed in NO_y are expected, a priori, for SO_2 in each plume intercept. In fact, the low upwind SO_2 mixing ratios observed along i0 (but not directly upwind) were followed by dramatic increases immediately downwind of the power plants that then decreased with each additional plume intercept further downwind (increase in plume age). This was consistently observed in all 6 investigated power plant plumes. The SO_2 levels downwind of a power plant increased due to stack emissions from coal combustion and then decreased with time as the air mass experienced dilution and SO_2 was exposed to chemical oxidation and deposition. The relative contributions of these processes to changes in SO_2 are beyond the scope of this paper, where the focus is on an analysis of rBC evolution that is clearly linked to strong power plant influences.

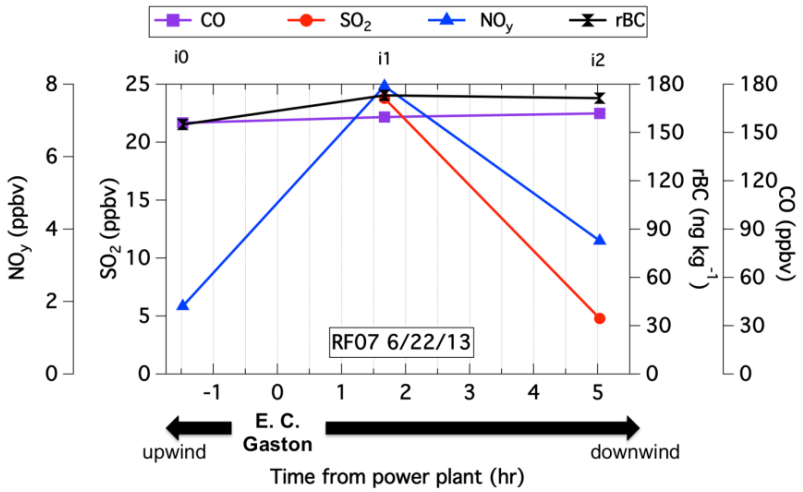

Figure 2. Volume mixing ratios of CO (squares, purple), SO_2 (circles, red), and NO_y (triangles, blue), and rBC mass mixing ratios (hour glass, black) in E. C. Gaston coal-fired power plume intercepts. Data points represent average values in each plume intercept. Negative times represent background measurements upwind of the power plant. The first intercept (i0) at −1.5 hr represents the measurement of the regional background upwind of the power plant, and the second and third intercepts represent measurements made 1.7 hr (i1) and 5 hr (i2) downwind of the power plant. SO_2 data was unavailable during i0.

3.2. Changes in microphysical properties of rBC in coal-fired power plant plumes

The number fraction of detected rBC-containing particles that were identified as coated (CF) increased in the plume simultaneously with the increase in fine (<1 μm) particle mass loadings (Figure 3, rBC concentration did not significantly vary). The AMS indicated increases only in the sulfate fraction; organic aerosol, nitrate aerosol, and ammonium all remained quite stable; this indicates that sulfate was most likely the strongest contributor to internal mixing with rBC. To the extent that non-sulfate species are contributing to the observed rBC-aging in the plumes, this would enhance the impacts attributed to sulfate. The CF in the plume was 1–5% higher than in the air masses surrounding them, which we attribute to in-plume chemistry forming additional coatings on the pre-existing rBC-containing particles. The rBC CF increased from 81 ± 1% in i0 upwind of the power plant to 83 ± 1% in i1 and to 86 ± 2% in i2.

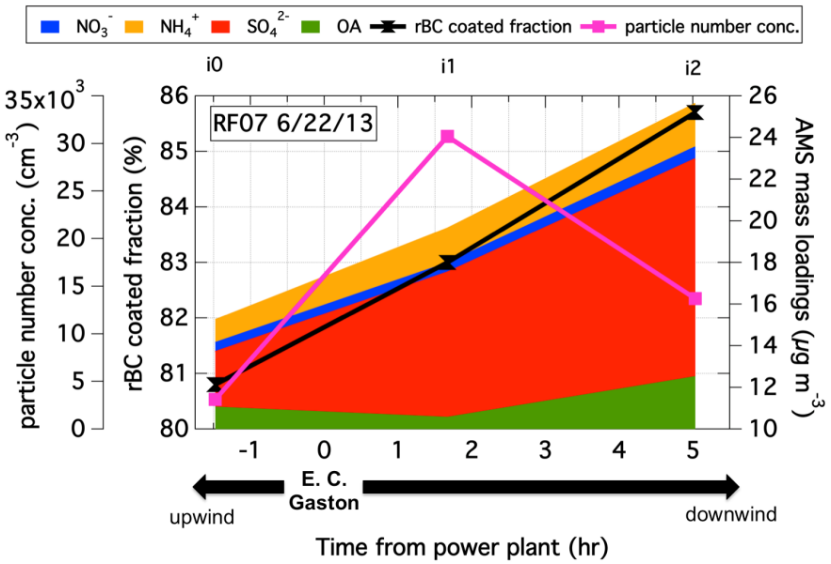

Figure 3. The fine particle number concentration (magenta), fraction of rBC that was identified as internally mixed (black), and the composition of fine particle mass plotted against the age of the E.C. Gaston coal-fired power plant plume. The fine particle composition measurements are stacked so that the top of the orange area represents the sum of the mass loadings of ammonium (NH_4^+, orange), nitrate (NO_3^-, blue), sulfate (SO_4^{2-}, red), and the organic aerosol (OA, green).

rBC coating thickness (CT) also increased in the aging plume. Figure 4 shows Gaussian fits to normalized histograms of CT from the upwind intercept, the two plume intercepts, and from the background air outside of the i2 intercept, labeled "i2 bkg". The i2 bkg represents air on each side of the i2 crossing within 30 s flight time of the plume. The mode of the Gaussian fit (x_0) to the estimated rBC CT distribution at i0 was 29 nm, which was close to the mission-average rBC CT value of 30 ± 15 nm standard deviation for rBC-containing aerosol populations upwind of all 6 investigated power plant plumes. In i1, at the plume age of 1.7 hr, the mode was x_0 = 36 nm, and by the age of 5 hr it had increased to x_0 = 42 nm. The x_0 for the estimated rBC CT in the i2 background, however, was x_0 = 37 nm, suggesting that most of the estimated rBC CT growth observed in i2 was

due to the contribution of more-aged regional rBC mixing in with the plume or common-mode aging independent of plume chemistry. Hence the average estimated rBC CT growth in the plume from 29 nm to 42 nm is an upper estimate for sulfate-driven aging of rBC in the plume.

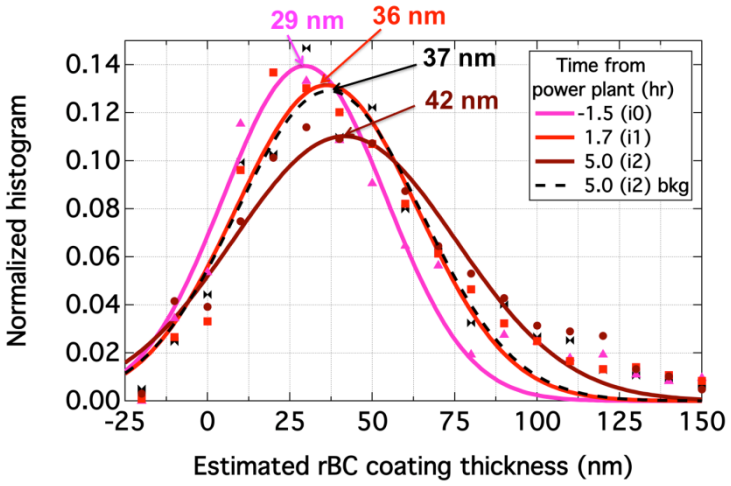

Figure 4. The changes in estimated rBC coating thicknesses of regional rBC population with age for the E. C. Gaston coal-fired power plant plume sampled June 22, 2013. The normalized histograms and the corresponding Gaussian fits of estimated coating thicknesses of 3–5 fg rBC cores (150–175 nm diameter equivalent) in each plume intercept and one plume intercept background are shown: i0 (magenta triangles), i0 fit (magenta line), i1 (red squares), i1 fit (red line), i2 (maroon circles), i2 fit (maroon line), i2 bkg (black bow tie), and i2 bkg fit (black dashed line). The area under each histogram was normalized to 1. The coating thicknesses were estimated by applying a Mie theory shell-core model to the measurements of the unperturbed rBC particle optical sizes and rBC core masses.

To exclude common-mode aging effects on the estimated rBC CT and CF sulfate-driven chemistry changes, the estimated rBC CT and CF in the plumes were corrected by subtracting the changes (assumed due to non-plume SOA production generally) observed near, but uninfluenced by, the plumes. The background values of rBC CF and CT in 30 s flight increments (~3.5 km spatial resolution) on each side of the plume along the flight path were averaged to provide a representative background, and its growth independent of the plume chemistry, and subtracted from the in-plume values to calculate the net estimated rBC CT and CF changes in the plume. These values for Gaston are shown in Figure 5. The whiskers represent uncertainty calculated by propagation of errors (1σ) associated with the in-plume and out-of-plume 30 s averages. With aging, the estimated rBC CT and CF increased at a slightly faster rate in the E. C. Gaston power plant plume than in the air mass surrounding the plume. Before influence of the plume, at i0, rBC CT and CF were very stable on the upwind leg, as expected. The net estimated rBC CT and CF were 5.9 ± 2.1 nm and 3.1 ± 1.4% at i1, and 4.6 ± 2.3 nm and 4.3 ± 1.6%, respectively, at i2. At i2, this growth corresponded to enhanced internally mixed mass of ~0.2 fg, or ~15% of the total internally mixed material on the rBC-containing particles treated here.

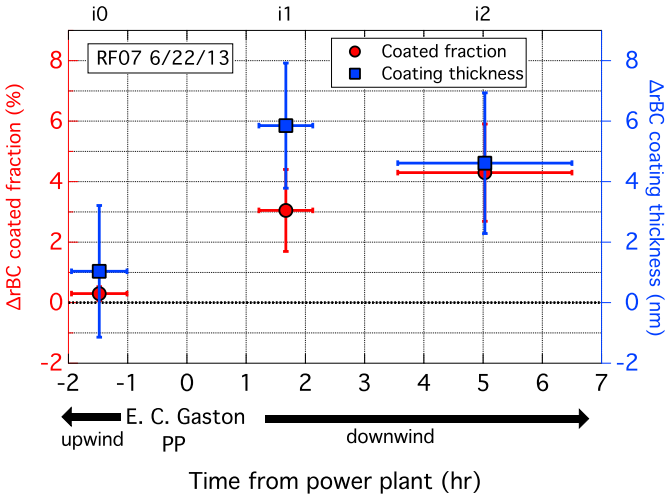

Figure 5. The average net changes in the estimated rBC CT (blue squares) and rBC CF (red circles) with the age of E. C. Gaston coal-fired power plant plume. The graph reflects the changes in estimated CT and CF for a population of rBC particles in 3–5 fg mass range relative to the changes outside of the plume along the flight path. Measurements from each side of the plume along the flight path in 30 s intervals were averaged to represent the background outside of the plume, which was mixing in with the plume as the it was undergoing dilution. The whiskers represent errors calculated by error propagation of errors (1σ) associated with the in-plume and out-of-plume 30 s averages. The dashed black line represents no net change in estimated rBC CF and the rBC CT.

Lower net estimated rBC CT and rBC CF increases were observed in intercepts of other power plant plumes (Figure 6). In some cases the values were even negative or decreasing with plume age, assumed to be a result of the limited signal-to-noise of our detection of these processes. The minimal coating increase is a consequence of multiple effects. First, most of the particle mass from sulfate-driven (or other) chemistry condenses or coagulates on the non-rBC-containing aerosol population; rBC-containing particles were generally a minor fraction (≤1%) of the total fine particle number in the air, and represented a similarly low fraction of the total aerosol surface area available to receive condensate. Secondly, the regional rBC-containing particles were already largely coated by OA components, consistent with estimated rBC CF and CT levels and large OA mass loadings observed in the background air masses. This is not surprising considering the large emissions of biogenic VOCs and the availability of solar radiation needed for photochemical oxidation are Southeast U.S. Potentially, a net increases in internal mixing of rBC due to plume-driven chemistry was overshadowed in some plumes by these processes.

If all sampled plume intercepts are considered, only a non-statistically relevant trend of increased estimated rBC CT and CF with increased with the age of the plume is observed, indicating that condensation of sulfate (and potentially other plume-chemistry products) was small. Compared to the rBC CT in the surrounding air mass, the net estimated rBC CT in power plant plumes was on average 2 ± 4 nm (±1 σ) and a median value of 3 nm. Similarly, the net rBC CF increased by 1.3 ± 1.3% (±1 σ) and the median value of 1.1%. The plumes were only investigated up to the age of ~5 hr due to the inherent difficulties in clearly identifying and characterizing older plumes that have intermixed via dilution with background air.

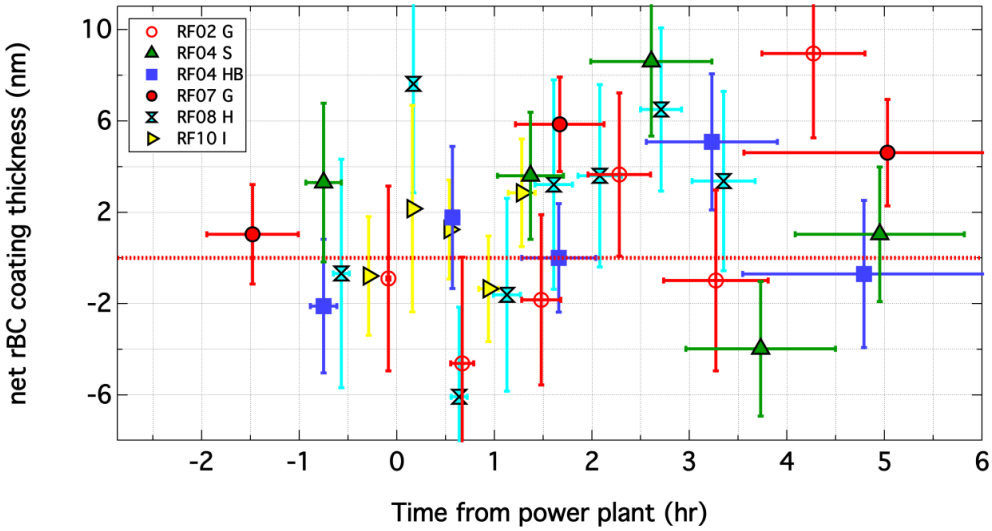

Figure 6. Changes in net estimated rBC coating thickness with plume age shown for all intercepts of all 6 power plant plumes (5 different power plants). The graph reflects the changes in estimated CT for a population of rBC particles in 3–5 fg mass range relative to the changes outside of the plume along the flight path. Measurements from each side of the plume along the flight path in 30 s intervals were averaged to represent the background outside of the plume, which was mixing in with the plume as it was undergoing dilution. The whiskers represent errors calculated by error propagation of errors (1σ) associated with the in-plume and out-of-plume 30 s averages.

The air-parcel history, including rBC mixing state, upwind of each power plant strongly affected the rates of coating thickness growth in plumes, as is evidenced by different aging on different days of observation of the same power plant plume. For example, the E. C. Gaston plume was characterized on both June 11 and 22. On the 11th, the wind was westerly from the direction of Tuscaloosa, AL providing fresher emissions of rBC-containing aerosol with lower (~25%) rBC CF of 0.62 and ~50% lower estimated rBC CT (14 nm) than on the 22nd. The mass loadings of OA were also ~40% lower. Moreover, the number concentration of fine particles in the plume on 06/11 was roughly one half of that on 06/22 after 5 hr, suggesting that there were less non-rBC particles to impede the condensation of sulfuric acid (with potential contributions from other plume-generated species) on rBC cores. Hence, the fresher, less internally mixed rBC population collected more coating mass in the power plant plume with a lower number of fine particles, as demonstrated in Figure 6.

3.3. The impact of coal-fired power plant plume chemistry on rBC optical properties in the Southeast U.S.

Although it is now clear that the sulfate condensed on to the rBC particle population is not a large contributor to the total coating thickness, it is useful to interpret the previous results in the context of rBC optics–and specifically rBC light absorption. This was done using a Mie theory core-shell optical model in conjunction with κ-Köhler theory to describe water uptake by the aerosol in ambient conditions [64]. Mie core-shell theory is widely used in calculations of light scattering and absorption by atmospheric particles, and in evaluations of laboratory and field

measurements [13,36,75–77]. The major limitation of the core-shell model is that it assumes that rBC-containing particles are composed of void-free and spherical core of rBC coated with a uniform layer of homogenous internally mixed material. Although ambient rBC particle have fractal characteristics, Qiu et al. [78] and China et al. [79] showed that with the development of organic coatings during atmospheric processing the rBC cores compact to a compact form, and that the consequent exposure to elevated humidity conditions results in near-spherical particles. These are typical conditions in summer-time Southeast U.S., which supports the use of the core-shell model here.

Our analysis was focused on the range of rBC-mass for which the SP2 was able to obtain the best statistics (3–5 fg rBC mass per particle). This range of mass is generally very near the mass-median diameter (i.e. typically half the total accumulation mode rBC mass occurs in particles with less than ~5 fg rBC mass, and half is in particles with more rBC mass than this). Over a limited rBC-mass range for which statistics are reasonable (up to ~10 fg), we do not observe significant trends in absorption enhancements due to coatings on rBC. Hence, we assume that our analysis is representative of the entire accumulation-mode population of rBC-containing particles.

The following microphysical conditions were considered in our calculations: 165 nm (~4 fg) rBC core that is initially coated with 30 nm of OA (κ = 0.1) takes up 2–9 nm of additional ammonium sulfate coating (κ = 0.53) as a direct result of power plant plume chemistry (Table 1). The rBC core size of d = 165 nm corresponds to the mode of the mass-size distribution of regional rBC population mixed into the 6 studied power plant plumes, and was within the range selected for the observations of rBC-containing particle optical size used to determine CTs. The average estimated rBC CT was determined to be 30 ± 15 nm upwind of all 6 investigated power plant plumes. The coatings on rBC particles were assumed to be completely composed of oxygenated OA. A density of 1.8 g cm^{-3} and complex refractive index of 2.26–1.26*i* were used for the rBC core. The real refractive indices 1.53 and 1.44 were used for ammonium sulfate and OA coatings respectively. The average, median, and maximum net estimated rBC CT enhancements observed in the investigated power plant plumes were 2 nm, 3 nm, and 9 nm, respectively; the average and median cases reflect very small changes; as such, their sensitivity to errors in assumed indecies of refraction (an indeed, of assumed composition) is negligible. Nitrate was excluded from the calculations because NO_3^- typically constituted only ~1% of the fine aerosol mass in power plant plumes.

Table 1. SENEX-relevant parameters used as an input to a Mie core-shell/κ–Köhler theory model framework for calculations of AE_{rBC}. RI = refractive index.

CASE	rBC core diameter	OA coating thickness	OA $\kappa/(NH_4)_2SO_4$ κ	OA RI/$(NH_4)_2SO_4$ RI	***$(NH_4)_2SO_4$ coating thickness***	RH
I	165 nm	30 nm	0.1/0.53	1.44/1.53	***2 nm***	50–95%
II	165 nm	30 nm	0.1/0.53	1.44/1.53	***3 nm***	50–95%
III	165 nm	30 nm	0.1/0.53	1.44/1.53	***6 nm***	50–95%
IV	165 nm	30 nm	0.1/0.53	1.44/1.53	***9 nm***	50–95%

We use Eq 1, below, to estimate the fraction (*F*) of the Southeast in which rBC could be influenced by power plant emissions within 5 hours aging:

$$F = A_P \cdot N_P / A_{SE} \quad (1)$$

where A_P is the estimated area of a single power plant plume after 5 hours (~180 sq. miles based on

the first E. C. Gaston plume observations), A_{SE} is the area of the Southeast, and N is the number coal- and oil-power plants that generate more than 25 MW yr^{-1} (166). Considering that the area of the entire Southeast U.S. (including LA, MS, AL, GA, FL, SC, NC, TN, AR, KY, WV, and VA) is 5.5×10^5 sq. miles, and assuming that the height of the PBL (for the purpose of this calculation defined as the mixed + transition layer [46]) is constant across the entire region, and assuming that the power plant plumes are rapidly mixed vertically throughout the PBL, only ~5% of the area of the Southeast U.S. is within the 5 hr old "plume cover".

To allow comparison to Stier et al. [14], in which the authors modeled the enhancements in column-integrated absorption optical depth, our calculations were extended above PBL, where typically 40% of rBC mass is located over the Southeast U.S. [45,46]. The atmospheric lifetime of rBC in our calculations was chosen to be 5 days to keep consistency with Stier et al. [14], this influenced the integrated impact of the additional coatings on the average column absorption of rBC-containing aerosol.

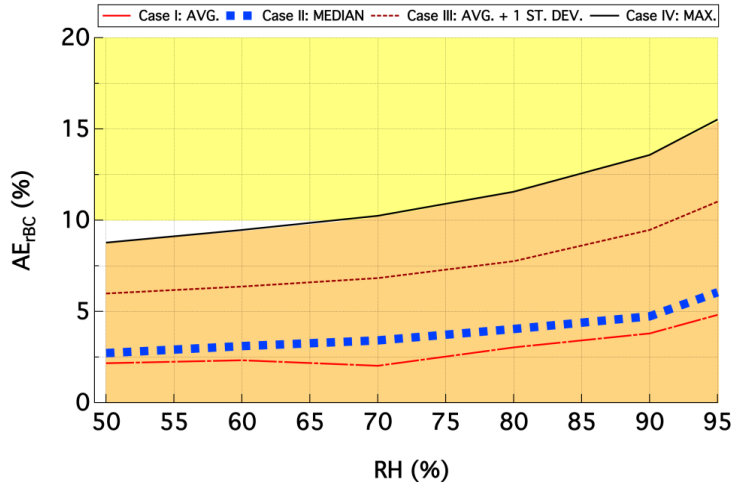

Figure 7. A comparison of rBC absorption enhancements, $AE_{rBC,}$ due to internal mixing of rBC with sulfate in the Southeast U. S. The range of values predicted by a climate-aerosol model in Stier et al. [14], for all anthropogenic sulfate is shown in yellow. The range of values calculated from rBC measurements during SENEX with κ-Köhler theory/ Mie theory core-shell model framework is shown in orange as a function of ambient relative humidity. The range was generated by using different coating thicknesses of ammonium sulfate on the mission-average rBC core size of 165 nm and OA coating thickness of 30 nm. The 4 lines/cases show the AE_{rBC} variability with RH when mission average (2 nm), mission median (3 nm), mission average +1 standard deviation (6 nm), and mission maximum (9 nm) net ammonium sulfate coating thicknesses were used in the calculations. Case I is our best estimate of the actual impact based on the observations made here.

The results of Mie/κ-Köhler theory framework calculations are shown in Figure 7. The enhancement in rBC absorption (AE_{rBC}: the calculated ratio of coated- to bare-rBC absorption) is shown as a function of relative humidity encountered during the study (50–95%). The total range of AE_{rBC} values calculated from our measurements is illustrated as solid orange fill. The range was

generated using different ammonium sulfate coating thicknesses in the calculations with the mission-average rBC core size of 165 nm and OA coating thickness of 30 nm (Table 1). The 4 cases illustrate the variability in AE_{rBC} as a function of RH when: (I) we use the mission average CT enhancement of 2 nm; this is our best estimate of the net enhancement; (II) we use the mission median CT enhancement of 3 nm; (III) we use the mission average CT + 1 standard deviation (6 nm), and (IV) we use the highest value observed for CT growth throughout the analysis, namely 9 nm. In each case we assume the plume-relevant added material is ammonium sulfate. The approximate range of AE_{rBC} for the total impacts of all anthropogenic SO_2 emissions globally, predicted by the ECHAM5-HAM climate-aerosol model described in Stier et al. [14], is shown in solid yellow fill yellow for comparison. We carried out sensitivity studies to test assumptions about core size, coating κ, and coating index of refraction had negligible effects on the results of the calculations.

We assumed that aging effects within highly concentrated power plant plumes would be associated with substantially higher associated coating enhancement than expected for large scale sulfate impacts under more general conditions (i.e., global scale evaluated over relatively coarse resolution). Nevertheless, the calculated best-estimate of AE_{rBC}, based on the measurements of rBC –containing particle optical size during the SENEX study, was lower than an estimate by ECHAM5-HAM, the climate-aerosol model described in Stier et al. [14], which simulated general conditions over global scales (200 km resolution, using all anthropogenic SO_2 emissions).

Based on Mie Shell-and-core theory, the addition of 2 to 3 nm of ammonium sulfate coating to a 165 nm rBC core originally coated by 30 nm OA in the power plant plume leads to regional additional AE_{rBC} due to sulfate uptake of ~ 2–6% (for 50–95% RH) in the Southeast U.S., which is ~5 times lower than the central prediction by the ECHAM5-HAM. In general, AE_{rBC} by sulfate coatings during SENEX were low because of the high levels of internal mixing of rBC with OA prior to exposure to coal-fired power plant plumes and the low number fractions of rBC-containing fine mode particles, such that surface area associated with rBC was a small fraction of the total available to receive condensates. In the presence of high levels of OA coatings (κ = 0.1) the addition of several nm of ammonium sulfate coatings (κ = 0.53) did not radically change the overall κ of the OA-$(NH_4)_2SO_4$ coating "mixture", which was generally <0.2 in our calculations. Thus, the water uptake and subsequent AE_{rBC} was significantly lower than what it would be if there were low levels of OA internally mixed with the rBC core. In addition, Lack and Cappa [76] previously showed that the AE_{rBC} can be impeded in the presence of internally mixed OA that can absorb light.

Two factors likely explain the stronger absorption enhancement simulated in Stier et al.: first, the representation of rBC in the model, and its transfer from a "bare" hydrophobic mode to an internally mixed mode (homogenously mixed with all mixed accumulation mode aerosol) after only the addition of a small amount of condensate. This occurs because the mixing state model of ECHAM-HAM (c.f. Table 1 in Stier et al., 2005) assumes that all rBC particles with coatings above a threshold (3 nm in Stier et al.) are transferred to the internally mixed accumulation mode, which significantly (and artificially) enhances the model simulated coating thickness. Secondly, the role of secondary organic aerosol in AE_{rBC} was neglected in the model treatment, which represented aerosol as emissions of primary organic matter, with rBC in which a fraction of freshly emitted rBC particles were treated as bare (i.e., completely water-inactive particles) that are grown to the accumulation mode hydrophilic particles by the addition of sulfate. Further, it is likely that all rBC particles freshly emitted from fossil fuel sources in the U.S. are associated with some degree of internal mixing, presumably from condensation of co-emitted semi-volatile organic vapors, certainly on the length

scale of dilution to the model grid box scale. Formation of additional OA coatings from VOC oxidation chemistry in the region such as Southeastern U.S., which is characterized by some of the highest VOC levels in the nation, would likely provide substantial coatings on rBC-containing particles. Addition of low levels of $(NH_4)_2SO_4$ to such rBC particles would have a minor impact on AE_{rBC} as explained above. However, an addition of even lower levels of $(NH_4)_2SO_4$ to bare, hydrophobic rBC particles would lead to large estimated AE_{rBC}. For example, if a 165 nm rBC particle initially coated with only 0.1 nm of hydrophobic OA ($\kappa = 0.01$) acquires 2 nm of $(NH_4)_2SO_4$ in a power plant plume, the resulting AE_{rBC} is ~17%, which is in the range of values predicted by [14]. In fact, sophisticated tracking of particle mixing, for example with a particle-resolved model like PART-MC [80], would be needed to resolve these phenomena. Based on empirical observations, we conclude that the effect of the addition of sulfate coatings on the rBC population in the summertime Southeastern U.S. has a small impact (2–6%) on the AE_{rBC} due to large levels of OA internally mixed with the rBC population.

4. Conclusion

During the SENEX field study in the Southeast U.S. in June and July of 2013, there was an opportunity to investigate changes in microphysical properties of background (aged) black carbon (rBC) particles downwind of coal-fired power plants. We have reported constraints on enhanced aging of rBC-containing particles from measurements in 6 plume intercepts of 5 power plants during 5 daytime flights. The aging was quantified by measurements of: (1) the fraction of rBC particles that could be identified as associated with internally mixed material (CF), and (2) the thickness of coatings (CT) on rBC-containing particles in the plumes relative to un-perturbed air. The background regional rBC aerosol population was internally mixed with large levels of oxygenated organic aerosol (OOA), likely due to high rates of volatile organic carbon (VOC) oxidation and condensation of organic chemicals of low to moderate volatility. The CF for the background rBC was over 80%, where, on average, 165 nm diameter rBC cores were coated with 30 ± 15 nm of (assumed) oxygenated OA. Fresher rBC emissions, for example from local cities, traffic, etc., were generally associated with thinner coatings. Power plant plume chemistry increased estimated rBC CT and rBC CF only slightly faster than background, with weak correlations to increased mass loadings of sulfate and ammonium. Thus, rBC aging in the plumes was indeed affected by sulfate chemistry. The rBC aging rates in power plant plumes were believed to be low because of the competition between rBC (<1% of total fine particle number) and non-rBC particles as sites for condensation and coagulation of sulfuric acid.

These direct measurements constrain predictions of the impact of aging of rBC by total anthropogenic SO_2 emissions (through sulfate-driven chemistry) on column-integrated aerosol absorption optical depth [14]. The observed net changes in estimated rBC CT were used in conjunction with Mie core-shell/κ-Köhler theory framework to show that the typical enhancements in absorption by rBC particles (AE_{rBC}) with the addition of internally mixed sulfate in the power plant plumes is likely in the 2–6% range. This type of processes, with condensation on an rBC particle population that is initially already largely internally mixed, requires a more sophisticated aerosol module version of ECHAM-HAM than used in Stier et al. [14] (such as was subsequently included [81,82]). In addition, the simplified representation of the aerosol mixing state in most aerosol microphysics schemes (except for models with significant complexity, such as [80]), in particular the assumption of internal mixing within modes or bins across climate model grid-scales,

can lead to unrealistic simulated microphysics including mixing states and associated absorption enhancements. Large amounts of OA internally mixed with rBC, with lower κ values (~0.1) compared to that of sulfate (~0.5), reduce the relative impact of the water uptake and consequent additional light absorption by rBC containing particles due to sulfate. Here, we expect that the derived aging time scales, the coating thickness, and the fraction of coated particles are the best constraints we can supply for future model developments from direct SP2 measurements of rBC-containing aerosol; naturally the continued development of this type of dataset is critical to provide constraints on model processes.

Acknowledgements

The authors thank Smyrna/Rutherford County Airport staff for their help and support during the study, and the entire NOAA WP-3D flight crew, science cohort, and support staff for their efforts in the field. We remember G. Hübler with fondness and gratitude for his assistance with mission logistics, and thank K. Aikin for his assistance with the programming and data analysis. P. Stier acknowledges support from the UK Natural Environment Research Council project GASSP (NE/J024252/1). The NOAA Black Carbon Group was supported in part by the NOAA Atmospheric Composition and Climate Program, the NASA Radiation Sciences Program, and the NASA Upper Atmosphere Research Program.

Conflicts of interest

All authors declare no conflicts of interest in this paper.

References

1. Hansen J, Sato M, Ruedy R (1997) Radiative forcing and climate response. *J Geophys Res* 102: 6831–6864.
2. Jacobson MZ (2001) Strong radiative heating due to the mixing state of black carbon in atmospheric aerosols. *Nature* 409: 695–697.
3. Ramanathan V, Carmichael G (2008) Global and regional climate changes due to black carbon. *Nature Geosci* 1: 221–227.
4. IPCC (2013) Climate Change 2013 The Physical Science Basis-Working Group I Contribution to the Fifth Assessment Report of the Intergovernmental Panel on Climate Change. *Cambridge University Press*.
5. Ramanathan V, Crutzen PJ, Lelieveld J, et al. (2001) Indian Ocean Experiment: An integrated analysis of the climate forcing and effects of the great Indo-Asian haze. *J Geophys Res* 106: 28371–28398.
6. Tripathi SN, Dey S, Tare V, et al. (2005) Aerosol black carbon radiative forcing at an industrial city in northern India. *Geophys Res Lett* 32, L08802.
7. Bond TC, Doherty SJ, Fahey DW, et al. (2013) Bounding the role of black carbon in the climate system: A scientific assessment. *J Geophys Res-Atmos* 118: 5380–5552.
8. Grieshop AP, Reynolds CCO, Kandlikar M, et al. (2009) A black-carbon mitigation wedge. *Nature Geosci* 2: 533–534.

9. Ramana MV, Ramanathan V, Feng Y, et al. (2010) Warming influenced by the ratio of black carbon to sulphate and the black-carbon source. *Nature Geosci* 3: 542–545.
10. Shindell D, Kuylenstierna JCI, Vignati E, et al. (2012) Simultaneously Mitigating Near-Term Climate Change and Improving Human Health and Food Security. *Science* 335: 183–189.
11. Nakicenovic N (2000) Greenhouse gas emissions scenarios. *Technol Forecast Soc Change* 65: 149–166.
12. Weingartner E, Burtscher H, Baltensperger U (1997) Hygroscopic properties of carbon and diesel soot particles. *Atmos Environ* 31: 2311–2327.
13. Schwarz JP, Perring AE, Markovic MZ, et al. (2015) Technique and theoretical approach for quantifying the hygroscopicity of black-carbon-containing aerosol using a single particle soot photometer. *J Aerosol Sci* 81: 110–126.
14. Stier P, Seinfeld JH, Kinne S, et al. (2006) Impact of nonabsorbing anthropogenic aerosols on clear-sky atmospheric absorption. *J Geophys Res-Atmos* 111, 2006JD007147.
15. Subramanian R, Kok GL, Baumgardner D, et al. (2010) Black carbon over Mexico: the effect of atmospheric transport on mixing state, mass absorption cross-section, and BC/CO ratios. *Atmos Chem Phys* 10: 219–237.
16. Chung SH, Seinfeld JH (2005) Climate response of direct radiative forcing of anthropogenic black carbon. *J Geophys Res-Atmos* 110.
17. Jacobson MZ (2002) Control of fossil-fuel particulate black carbon and organic matter, possibly the most effective method of slowing global warming. *J Geophys Res-Atmos* 107, 2001JD01376.
18. Lesins G, Chylek P, Lohmann U (2002) A study of internal and external mixing scenarios and its effect on aerosol optical properties and direct radiative forcing. *J Geophys Res* 107, 2001JD000973.
19. Martins JV, Artaxo P, Liousse C, et al. (1998) Effects of black carbon content, particle size, and mixing on light absorption by aerosols from biomass burning in Brazil. *J Geophys Res* 103: 32041–32050.
20. Moffet RC, Prather KA (2009) In-situ measurements of the mixing state and optical properties of soot with implications for radiative forcing estimates. *P Natl Acad SCI USA* 106: 11872–11877.
21. Lim S, Lee M, Kim SW, et al. (2018) Sulfate alters aerosol absorption properties in East Asian outflow. *Nat Sci Rep* 8: 5172.
22. Wu Y, Cheng I, Zheng L, et al. (2016) Black carbon radiative forcing at TOA decreased during aging. *Nat Sci Rep* 6: 38592.
23. Cooke WF, Liousse C, Cachier H, et al. (1999) Construction of a 1 degrees x 1 degrees fossil fuel emission data set for carbonaceous aerosol and implementation and radiative impact in the ECHAM4 model. *J Geophys Res* 104: 22137–22162.
24. Croft B, Lohmann U, von Salzen K (2005) Black carbon ageing in the Canadian Centre for Climate modelling and analysis atmospheric general circulation model. *Atmos Chem Phys* 5: 1931–1949.
25. Koch D (2001) Transport and direct radiative forcing of carbonaceous and sulfate aerosols in the GISS GCM. *J Geophys Res* 106: 20311–20332.
26. Riemer N, Vogel H, Vogel B (2004) Soot aging time scales in polluted regions during day and night. *Atmos Chem Phys* 4: 1885–1893.

27. Lund M, Berntsen K, Samset BH (2017) Sensitivity of black carbon concentrations and climate impact to aging and scavenging in OsloCTM2–M7. *Atmos Chem Phys* 17: 6003–6022.
28. Bond TC, Bergstrom RW (2006) Light absorption by carbonaceous particles: An investigative review. *Aerosol Sci Tech* 40: 27–67.
29. Bond TC, Habib G, Bergstrom RW (2006) Limitations in the enhancement of visible light absorption due to mixing state. *J Geophys Res-Atmos* 111, 2006JD007315.
30. Cross ES, Onasch TB, Ahern A, et al. (2010b) Soot Particle Studies—Instrument Inter-Comparison—Project Overview. *Aerosol Sci Tech* 44: 592–611.
31. Myhre G (2009) Consistency Between Satellite-Derived and Modeled Estimates of the Direct Aerosol Effect. *Science* 325: 187–190.
32. Schnaiter M, Linke C, Mohler O, et al. (2005) Absorption amplification of black carbon internally mixed with secondary organic aerosol. *J Geophys Res-Atmos* 110, 2005JD006046.
33. Schwarz JP, Spackman JR, Fahey DW, et al. (2008) Coatings and their enhancement of black carbon light absorption in the tropical atmosphere. *J Geophys Res* 113, 2007JD009042.
34. Lack DA, Langridge JM, Bahreini R, et al. (2012) Brown carbon and internal mixing in biomass burning particles. *P Natl Acad Sci USA* 109: 14802–14807.
35. Wang Q, Huang RJ, Cao J, et al. (2014) Mixing state of black carbon aerosol in a heavily polluted urban area of China: Implications for light absorption enhancement. *Aerosol Sci Tech* 48: 689–697.
36. Cappa CD, Onasch TB, Massoli P, et al. (2012) Radiative Absorption Enhancements Due to the Mixing State of Atmospheric Black Carbon. *Science* 337: 1078–1081.
37. Lan ZJ, Huang XF, Yu KY, et al. (2013) Light absorption of black carbon aerosol and its enhancement by mixing state in an urban atmosphere in South China. *Atmos Environ* 69: 118–123.
38. Fierce L, Riemer N, Bond TC (2015) Explaining variance in black carbon's aging timescale. *Atmos Chem Phys* 15: 3173–3191.
39. Warneke C, Trainer M, de Gouw, et al. (2016) Instrumentation and measurement strategy for the NOAA SENEX aircraft campaign as part of the Southeast Atmosphere Study 2013. *Atmos Meas Tech* 9: 3063–3093.
40. Attwood AR, Washenfelder RA, Brock CA, et al. (2014) Trends in sulfate and organic aerosol mass in the Southeast U.S.: Impact on aerosol optical depth and radiative forcing. *Geophys Res Lett* 41: 7701–7709.
41. Brock CA, Wagner NL, Anderson BE, et al. (2015) Aerosol optical properties in the southeastern United States in summer–Part 2: Sensitivity of aerosol optical depth to relative humidity and aerosol parameters. *Atmos Chem Phys Discuss* 15: 31471–31499.
42. Brock CA, Wagner NL, Anderson BE, et al. (2015b) Aerosol optical properties in the southeastern United States in summer–Part 1: Hygroscopic growth. *Atmos Chem Phys Discuss* 2015: 25695–25738.
43. Hand JL, Copeland SA, Day DE, et al. (2011) Spatial and Seasonal Patterns and Temporal Variability of Haze and its Constituents in the United States: Report V. Colorado State University, Fort Collins CO, 2011.
44. Hidy GM, Blanchard CL, Baumann K, et al. (2014) Chemical climatology of the southeastern United States, 1999–2013. *Atmos Chem Phys* 14: 11893–11914.

45. Kim PS, Jacob DJ, Fisher JA, et al. (2015) Sources, seasonality, and trends of southeast US aerosol: an integrated analysis of surface, aircraft, and satellite observations with the GEOS-Chem chemical transport model. *Atmos Chem Phys* 15: 10411–10433.
46. Wagner NL, Brock CA, Angevine WM, et al. (2015) In situ vertical profiles of aerosol extinction, mass, and composition over the southeast United States during SENEX and SEAC4RS: observations of a modest aerosol enhancement aloft. *Atmos Chem Phys* 15: 7085–7102.
47. Washenfelder RA, Attwood AR, Brock CA, et al. (2015) Biomass burning dominates brown carbon absorption in the rural southeastern United States. *Geophys Res Lett* 42: 653–664.
48. Miller BG (2010) Clean Coal Engineering Technology. *Elsevier Inc, Oxford*, 375–481.
49. Zhang Y, Vijayaraghavan K, Wen XY, et al. (2009) Probing into regional ozone and particulate matter pollution in the United States: 1. A 1 year CMAQ simulation and evaluation using surface and satellite data. *J Geophys Res-Atmos* 114: 2009JD0011898.
50. Jacob DJ (1999) *Introduction to Atmospheric Chemistry*, Princeton University Press, Princeton, NJ.
51. Kulmala M, Kerminen VM (2008) On the formation and growth of atmospheric nanoparticles. *Atmos Res* 90: 32–150.
52. Junkermann W, Vogel B, Sutton MA (2011) The climate penalty for clean fossil fuel combustion. *Atmos Chem Phys* 11: 12917–12924.
53. Junkermann W, Hagemann R, Vogel B (2011b) Nucleation in the Karlsruhe plume during the COPS/TRACKS-Lagrange experiment. *Q J Roy Meteor Soc* 137: 267–274.
54. Lonsdale CR, Stevens RG, Brock CA, et al. (2012) The effect of coal-fired power-plant SO2 and NOx control technologies on aerosol nucleation in the source plumes. *Atmos Chem Phys* 12: 11519–11531.
55. Petzold A, Ogren JA, Fiebig M, et al. (2013) Recommendations for reporting "black carbon" measurements. *Atmos Chem Phys* 13: 8365–8379.
56. Schwarz JP, Spackman JR, Gao RS, et al. (2010) The Detection Efficiency of the Single Particle Soot Photometer. *Aerosol Sci Tech* 44: 612–628.
57. Schwarz JP, Gao RS, Spackman JR, et al. (2008) Measurement of the mixing state, mass, and optical size of individual black carbon particles in urban and biomass burning emissions. *Geophys Res Lett* 35, L13810, 2008GL033968.
58. Cross ES, Onasch TB, Ahern A, et al. (2010a) Intercomparison study of black carbon measurements. Abstracts of Papers of the American Chemical Society, 1155 16TH ST, NW, WASHINGTON, DC 20036 USA: AMER CHEMICAL SOC, 240.
59. Schwarz JP, Gao RS, Fahey DW, et al. (2006) Single-particle measurements of midlatitude black carbon and light-scattering aerosols from the boundary layer to the lower stratosphere. *J Geophys Res* 111(D16), D16207, 2006JD007076.
60. Murphy DM, Cziczo DJ, Hudson PK, et al. (2004) Particle generation and resuspension in aircraft inlets when flying in clouds. *Aerosol Sci Tech* 38: 400–408.
61. Lance S, Brock CA, Rogers D, et al. (2010) Water droplet calibration of the Cloud Droplet Probe (CDP) and in-flight performance in liquid, ice and mixed-phase clouds during ARCPAC. *Atmos Meas Tech* 3: 1683–1706.
62. Baumgardner D, Popovicheva O, Allan J, et al. (2012) Soot reference materials for instrument calibration and intercomparisons: a workshop summary with recommendations. *Atmos Meas Tech* 5: 1869–1887.

63. Moteki N, Kondo Y (2010) Dependence of Laser-Induced Incandescence on Physical Properties of Black Carbon Aerosols: Measurements and Theoretical Interpretation. *Aero Sci Technol* 44: 663–675.
64. Gysel M, Laborde M, Olfert JS, et al. (2011) Effective density of Aquadag and fullerene soot black carbon reference materials used for SP2 calibration. *Atmos Meas Technol* 4: 2851–2858.
65. Gao RS, Schwarz JP, Kelly KK, et al. (2007) A novel method for estimating light-scattering properties of soot aerosols using a modified single-particle soot photometer. *Aerosol Sci Tech* 41: 125–135.
66. Petters MD, Kreidenweis SM (2007) A single parameter representation of hygroscopic growth and cloud condensation nucleus activity. *Atmos Chem Phys* 7: 1961–1971.
67. Bahreini R, Ervens B, Middlebrook AM, et al. (2009) Organic aerosol formation in urban and industrial plumes near Houston and Dallas, Texas. *J Geophys Res-Atmos* 114, D00F16, 2008JD011493.
68. Liao J, Brock CB, Murphy DM, et al. (2017) Single-particle measurements of bouncing particles and in situ collection efficiency from an airborne aerosol mass spectrometer (AMS) with light-scattering detection. *Atmos Meas Tech* 10: 3801–3820.
69. Brock CA, Schroder F, Karcher B, et al. (2000) Ultrafine particle size distributions measured in aircraft exhaust plumes. *J Geophys Res* 105: 26555–26567.
70. Brock C A, Cozic J, Bahreini R, et al. (2011) Characteristics, sources, and transport of aerosols measured in spring 2008 during the aerosol, radiation, and cloud processes affecting Arctic Climate (ARCPAC) Project. *Atmos Chem Phys* 11: 2423–2453.
71. Pollack IB, Lerner BM, Ryerson TB (2010) Evaluation of ultraviolet light-emitting diodes for detection of atmospheric NO2 by photolysis-chemiluminescence. *J Atmos Chem* 65: 111–125.
72. Ryerson TB, Williams EJ, Fehsenfeld FC (2000) An efficient photolysis system for fast-response NO2 measurements. *J Geophys Res* 105: 26447–26461.
73. Ryerson TB, Huey LG, Knapp K, et al. (1999) Design and initial characterization of an inlet for gas-phase NOy measurements from aircraft. *J Geophys Res* 104: 5483–5492.
74. Holloway JS, Jakoubek RO, Parrish DD, et al. (2000) Airborne intercomparison of vacuum ultraviolet fluorescence and tunable diode laser absorption measurements of tropospheric carbon monoxide. *J Geophys Res* 105: 24251–24261.
75. Jacobson MZ (2012) Investigating cloud absorption effects: Global absorption properties of black carbon, tar balls, and soil dust in clouds and aerosols. *J Geophys Res-Atmos* 117, 2011JD017218.
76. Lack DA, Cappa CD (2010) Impact of brown and clear carbon on light absorption enhancement, single scatter albedo and absorption wavelength dependence of black carbon. *Atmos Chem Phys* 10: 4207–4220.
77. Saleh R, Robinson ES, Tkacik DS, et al. (2014) Brownness of organics in aerosols from biomass burning linked to their black carbon content. *Nature Geosci* 7: 647–650.
78. Qiu C, Khalizov AF, Zhang R (2012) Soot aging from OH-initiated oxidation of toluene. *Environ Sci Technol* 46: 9464–9472.
79. China S, Scarnato B, Owen RC, et al. (2015) Morphology and mixing state of aged soot particles at a remote marine free troposphere site: Implications for optical properties. *Geophys Res Lett* 42: 1243–1250.
80. Reimer N, West M, Zaveri RA, et al. (2009) Simulating the evolution of soot mixing state with a particle-resolved aerosol model. *J Geophys Res* 114(D9), 2008JD011073.

81. O'Donnel D, Tsigaridis K, Feichter J (2011) Estimating the direct and indirect effects of secondary organic aerosols using ECHAM5-HAM. *Atmos Chem Phys* 11: 8635–8559.
82. Zhang K, O'Donnell D, Kazil J, et al. (2012) The global aerosol-climate model ECHAM-HAM, version 2: sensitivity to improvements in process representations. *Atmos Chem Phys* 12: 8911–8949.

AIMS Press